Surface Science Letters

Structure, band offsets and photochemistry at epitaxial α-Cr₂O₃/α-Fe₂O₃ heterojunctions

S.A. Chambers [a,*], J.R. Williams [a], M.A. Henderson [a], A.G. Joly [a], M. Varela [b], S.J. Pennycook [b]

[a] Pacific Northwest National Laboratory, Fundamental Science Division, 3335 Q Avenue, Richland 99352 WA, USA
[b] Oak Ridge National Laboratory, Oak Ridge, TN, USA

Abstract

We test the hypothesis that electron–hole pair separation following light absorption enhances photochemistry at oxide/oxide heterojunctions which exhibit a type II or staggered band alignment. We have used hole-mediated photo-decomposition of trimethyl acetic acid chemisorbed on surfaces of heterojunctions made from epitaxial α-Cr₂O₃ on α-Fe₂O₃(0001) to monitor the effect of UV light of wavelength 385 nm (3.2 eV) in promoting photodissociation. Absorption of photons of energies between the bandgaps of α-Cr₂O₃ (E_g = 4.8 eV) and α-Fe₂O₃ (E_g = 2.1 eV) is expected to be strong only in the α-Fe₂O₃ layer. The staggered band alignment should then promote the segregation of holes (electrons) to the α-Cr₂O₃ (α-Fe₂O₃) layer. Surprisingly, we find that the α-Cr₂O₃ surface alone promotes photodissociation of the molecule at $h\nu$ = 3.2 eV, and that any effect of the staggered band alignment, if present, is masked. We propose that the inherent photoactivity of the α-Cr₂O₃(0001) surface results from the creation of bound excitons in the surface which destabilize the chemisorption bond in the molecule, resulting in photodecomposition.
© 2005 Published by Elsevier B.V.

Keywords: Photocatalysis; Heterojunctions; Epitaxial

1. Introduction

Heterogeneous photocatalysis on oxide surfaces represents a rich field of study that is both funda- mentally interesting and important for a variety of technologies. For example, photocleaning is a rap- idly developing technology in which electron–hole pair creation at the surface of a thin TiO₂ coating on window glass results in photochemical decom- position of adsorbed organic contaminants. The fundamentals of this and related processes are not only fascinating, but also essential to under-

* Corresponding author. Tel.: +1 509 376 1766; fax: +1 509 376 5106.
  E-mail address: sa.chambers@pnl.gov (S.A. Chambers).

S.A. Chambers et al. / Surface Science xxx (2005) xxx–xxx

stand in order to advance the technology [1]. The heterogeneous photocatalytic activity of TiO_2 has been studied in some detail [2]. That of other oxides, such as α-Cr_2O_3 and α-Fe_2O_3, has generally been avoided. Thiel et al. [3] investigated the role of surface vibrations on the photochemistry of NO on a thin epitaxial film of α-$Cr_2O_3(0001)$ grown on Cr(110). The photochemistry of Fe_2O_3 particles in aqueous solutions [4,5] and in the gas phase [6] has also been studied to a limited extent. One reason the oxides of Fe and Cr have generally been avoided is that conventional wisdom suggests that d-states in the band gap of these materials may act as trapping sites and/or electron–hole (e^-/h^+) pair recombination centers, thereby reducing heterogeneous photocatalytic activity.

In principle, e^-/h^+ pair lifetimes can be enhanced by spatial separation of charges via a heterojunction in which the band edges are staggered. While some work has been done on the photocatalytic activity of α-Fe_2O_3 in a heterojunction structure, this work primarily involved small particles in solution consisting of at least two layers of different oxides [7]. This work, while more reflective of real-world conditions, nevertheless does little to yield insight into photochemical mechanisms and the impact of the heterojunction structure. A multitude of experimental variables, many of which are uncontrolled, preclude determination of specific cause-and-effect relationships. To gain fundamental understanding it is often necessary to simplify and define the system sufficiently well that the number of experimental variables is limited. To this end, we have examined the effect of oxide heterojunction formation on photocatalytic activity using epitaxial films of α-Cr_2O_3 and α-Fe_2O_3 grown and studied entirely in a UHV environment. The α-Cr_2O_3/α-$Fe_2O_3(0001)$ system was chosen because it is readily grown by oxygen plasma assisted molecular beam epitaxy, and exhibits a staggered, albeit noncommutative band alignment [8]. A noncommutative band alignment is one in which the band offset for A on B is different from that of B on A. The noncommutativity was tentatively assigned to a difference in interface structure for α-Cr_2O_3 grown on α-Fe_2O_3 compared to α-Fe_2O_3 grown on α-Cr_2O_3, with the resulting change in interface dipole. Subsequent theoretical calculations supported this conclusion and yielded plausible differences in interface structure that would lead to the observed band offset noncommutativity [9]. Inasmuch as staggered semiconductor band alignments are known to be effective at separating e^-/h^+ pairs created by the absorption of sub-bandgap light [10], we investigate in the present work the hypothesis that photochemistry can be carried out to a greater extent on such a heterojunction than is possible on the surface of either material in isolation.

The remainder of the paper is organized as follows. Following experimental details in Section 2, we present in Section 3 new results on the abruptness of the interface and the dependence of band offset on growth temperature. In addition, we present new results which refine and strengthen the band offset analysis discussed originally in Ref. [8]. In Section 4, we discuss hole-mediated photodecomposition of trimethyl acetate (TMA) adsorbed on α-Cr_2O_3/α-Fe_2O_3 heterojunctions and the associated free surfaces of the pure materials, and we summarize in Section 5.

2. Experimental

Film growth by oxygen plasma assisted molecular beam epitaxy (OPAMBE), X-ray photoelectron spectroscopy (XPS) measurements, and all photodesorption experiments were performed in separate custom ultrahigh vacuum (UHV) chambers connected by a custom UHV sample transfer system [11]. All epitaxial films and heterojunctions were grown on α-$Al_2O_3(0001)$ substrates cleaned by room temperature exposure to activated oxygen for thirty minutes. Reference surfaces of α-Cr_2O_3 film were grown directly on α-$Al_2O_3(0001)$, and were typically 600 Å thick. Reference surfaces of α-Fe_2O_3 film were typically 1100 Å thick, and were grown on a 100 Å-thick α-Cr_2O_3 buffer layer to mitigate the large in-plane lattice mismatch between α-Fe_2O_3 and the α–Al_2O_3 substrate ($\Delta a/a$ = 5.80% and 3.36% for α-Fe_2O_3/α-$Al_2O_3(0001)$ and α-Cr_2O_3/α-$Al_2O_3(0001)$, respectively). Heterojunctions consisting of a few to several monolayers (ML) of α-Cr_2O_3 were prepared on reference surfaces of α-$Fe_2O_3(0001)$, as described above. In situ

SUSC 15669

1 June 2005 Disk used

ARTICLE IN PRESS

No. of Pages 11, DTD = 5.0.1

SURFACE SCIENCE
LETTERS

S.A. Chambers et al. / Surface Science xxx (2005) xxx–xxx

3

129 thickness calibration of the Cr_2O_3 ML was
130 achieved by relating the period of reflection high-
131 energy electron diffraction (RHEED) intensity
132 oscillations observed during the growth of the
133 Cr_2O_3 buffer layer with the Cr flux measured by
134 atomic absorption (AA) spectroscopy [8]. The
135 Cr_2O_3 films were then grown for a period of time
136 corresponding to some multiple of the RHEED
137 intensity oscillation period ($\sim$15 s) at the same
138 AA value. The substrate temperature was varied
139 from 500 to 800 °C.
140   Immediately after film growth and before dos-
141 ing with trimethyl acetic acid (TMAA), XPS with
142 monochromatic AlKα X-rays was carried out at
143 a take-off angle (θ_t) of 12° relative to the surface
144 plane to check for surface carbon contamination
145 and to identify the surface termination. α-
146 $Fe_2O_3(0001)$ films grown under OPAMBE condi-
147 tions are Fe-terminated [12], while α-Cr_2O_3
148 (0001) films can be either Cr or chromyl-termi-
149 nated [13], depending on the amount of oxygen
150 present in the chamber during cool down follow-
151 ing growth [14]. Chromyl termination of the
152 $Cr_2O_3(0001)$ surface can be detected as a high-
153 binding energy shoulder on the lattice oxygen peak
154 in a high-resolution O 1s XPS spectrum collected
155 at grazing emission [14]. Charge neutralization
156 by low-energy (1–2 eV) electron bombardment
157 from a flood gun was necessary during XPS be-
158 cause of the insulating nature of these materials.
159 Thus, the measured binding energies were not
160 absolute as measured, and all spectra were ad-
161 justed so the lattice O 1s binding energy was
162 530.0 eV.
163   TMA C and O 1s core-level spectra were mea-
164 sured after dosing with TMAA, but prior to UV
165 irradiation and photodesorption measurements.
166 These measurements were then repeated after UV
167 irradiation. The stability of the adsorbed molecule
168 with respect to X-ray flux and flood gun bombard-
169 ment in XPS was found to be excellent, even for
170 several hours of analysis. The standard TMAA
171 dose ranged from 12 L for Fe_2O_3 up to 1200 L
172 for Cr_2O_3, and was found to result in saturation
173 of the different surfaces. Here, we have assumed
174 an enhancement factor of $\sim$100 from the direc-
175 tional doser we employed. All dosing, analysis
176 and photodesorption experiments were performed

177 with the specimen at $\sim$300 K. A chopped 100 W
178 Hg arc lamp with a water-filled infrared filter, a
179 collimating lens, and a cut-off filter which removed
180 all emission lines of wavelength less than 385 nm
181 was used as the photoexcitation source. After pass-
182 ing through the lens, the lamp spot size was $\sim$1 cm
183 in diameter, matching the sample size. TMA pho-
184 todesportion was monitored in real-time using a
185 shielded residual gas analyzer.
186   Electron microscopy observations and electron
187 energy loss spectroscopy (EELS) were carried out
188 *ex situ* in a scanning transmission electron micro-
189 scope (STEM) VG Microscopes HB501UX oper-
190 ated at 100 kV and equipped with a Nion
191 aberration corrector and a parallel electron energy
192 loss spectrometer. This microscope is capable of
193 routinely achieving a spatial resolution of
194 0.13 nm. Cross sectional samples for STEM were
195 prepared by conventional methods: grinding, dim-
196 pling and Ar ion milling at 5 kV.

3. Interface abruptness and band offsets   197

198   The common corundum crystal structure of α-
199 Cr_2O_3 and α-Fe_2O_3 together with the fact that
200 Cr(III) and Fe(III) have similar ionic radii suggests
201 that α-Cr_2O_3 and α-Fe_2O_3 should exhibit a high de-
202 gree of miscibility. However, we have found that
203 the interface between these two materials is rather
204 abrupt. We show in Fig. 1 STEM images of a α-
205 Cr_2O_3/α-Fe_2O_3/α- Cr_2O_3/α-$Al_2O_3(0001)$ multilayer
206 stack grown at 600 °C. The low-resolution image
207 shown in Fig. 1a reveals a high degree of flatness
208 for each film, as well as an apparent abruptness
209 of each interface. The higher resolution images in
210 Fig. 1b and c reveal the cation rows in three mate-
211 rials, and the contrast is suggestive of abrupt inter-
212 faces. In Fig. 2a we show electron energy loss
213 spectra as a function of position along a line nor-
214 mal to the α-Cr_2O_3/α-Fe_2O_3 interface. The Cr $L_{2,3}$
215 edge loss feature diminishes and the Fe $L_{2,3}$ edge
216 feature grows as the interface is crossed in passing
217 from α-Cr_2O_3 to α-Fe_2O_3. The integrated areas un-
218 der the two metal L-edge loss features are plotted
219 against distance along the normal line in Fig. 2b.
220 From these data, the *apparent* width of the inter-
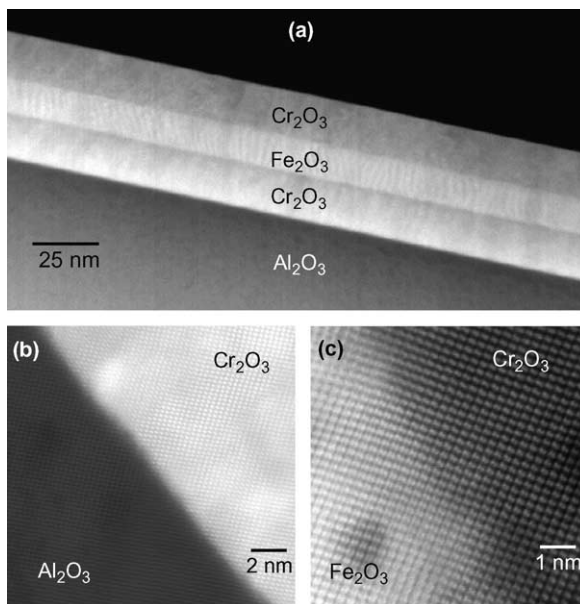221 face is $\sim$10 Å, or 4 ML of M_2O_3. However, there

Fig. 1. STEM images of an epitaxial α-Cr$_2$O$_3$/α-Fe$_2$O$_3$/α-Cr$_2$O$_3$/α-Al$_2$O$_3$(0001) layered specimen.

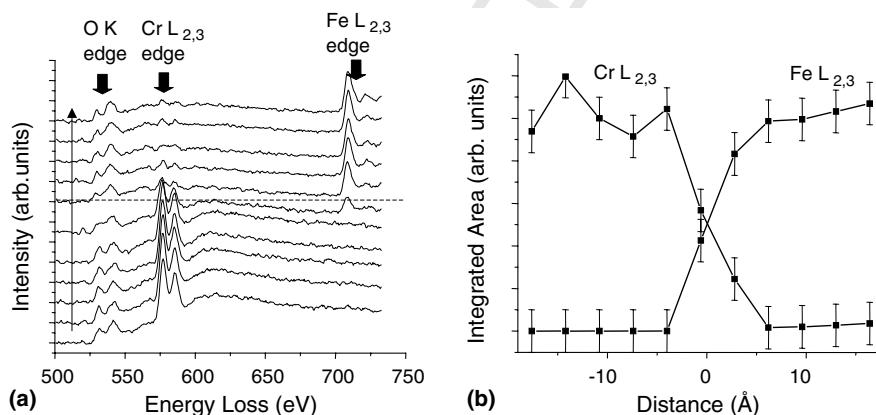

Fig. 2. (a) Energy loss spectra taken along a line normal to the interface of α-Cr$_2$O$_3$ and α-Fe$_2$O$_3$ and (b) integrated areas under the Cr L$_{2,3}$ and Fe L$_{2,3}$ loss features as a function of distance from the interface.

is a finite interaction volume for the electron beam, so the actual interface width is less than 10 Å. From these data, along with the Z-contrast images in Fig. 1, we conclude that the interface is quite abrupt, with intermixing extending to no more than ±1 ML from the interface. This result is crucial because intermixing defines the composition and structure of the interface and, thus, the interface dipole potential, which is one term in the band offset.

The valence band offset can be determined from core-level and valence band binding energies for α-Cr$_2$O$_3$, α-Fe$_2$O$_3$, and heterojunctions (HJ) of the two from the formula,

$$\Delta E_v = (E_{Fe3p} - E_v)_{Fe_2O_3} - (E_{Cr3p} - E_v)_{Cr_2O_3} - (E_{Fe3p} - E_{Cr3p})_{HJ} \qquad (1)$$

The subscript HJ refers to the heterojunction consisting of α-Cr$_2$O$_3$ on α-Fe$_2$O$_3$. We plot in

SUSC 15669

1 June 2005 Disk used

ARTICLE IN PRESS

No. of Pages 11, DTD = 5.0.1

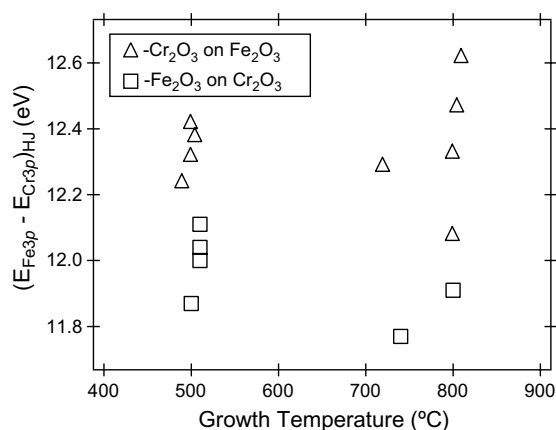SURFACE SCIENCE
LETTERS

S.A. Chambers et al. / Surface Science xxx (2005) xxx–xxx

5

Fig. 3. Shallow core-level binding energy difference $(E_{Fe3p} - E_{Cr3p})$ vs. growth temperature for epitaxial α-Cr$_2$O$_3$/α-Fe$_2$O$_3$ heterojunctions. The valence band offset depends linearly on this quantity.

Fig. 3 the quantity $(E_{Fe3p} - E_{Cr3p})_{HJ}$ for hetero- 240
junctions, in which the thickness of the top layer 241
was ∼15 Å, as a function of growth temperature. 242
As seen in Fig. 3, the HJs grown at 500 °C, for 243
which the interfaces are as abrupt as those shown 244
in Figs. 1 and 2, the $(E_{Fe3p} - E_{Cr3p})_{HJ}$ values tend 245
to fall into narrow bands centered at 12.00 ± 0.15 246
and 12.35 ± 0.10 eV for the two kinds of HJs, in 247
excellent agreement with previous results [8]. 248
Increasing the growth temperature to 800 °C 249
causes the $(E_{Fe3p} - E_{Cr3p})_{HJ}$ values to disperse 250
slightly more, in keeping with expected slightly 251
greater extents of intermixing, and less well-con- 252
trolled interface composition at the higher growth 253
temperature. Nevertheless, the noncommutativity 254
in the valence band offset is still present at a 255
growth temperature of 800 °C, revealing that dif- 256
ferences in interface composition and structure re- 257
main in tact for the two growth sequences. 258
Previous theoretical calculations suggest that 259
growing Cr$_2$O$_3$ on Fe$_2$O$_3$ results in the formation 260
of a "split-metal" interface, as depicted in Fig. 7 261
[9]. In contrast, growth of the inverted interface 262
was predicted to result in an "oxygen-divided" 263
interface, in which a close-packed layer of O an- 264
ions defines the interface, and two 1/3 ML of Fe 265
(Cr) are above (below) this O layer. Unfortunately, 266
it is not possible to distinguish between these two 267
interface structures with current TEM technology 268

due to the similarity in atomic number for Cr 269
and Fe. 270
A recent exchange in the literature raised the is- 271
sue of how best to determine the valence band 272
maximum (VBM) from XPS measurements of 273
the valence band spectra of oxides. Accurate deter- 274
mination of the VBM (E_v in Eq. (1)) is of critical 275
importance to finding the quantities $(E_{Fe3p} - E_v)_{Fe}$ 276
and $(E_{Cr3p} - E_v)_{Cr}$ with sufficient accuracy to ob- 277
tain accurate values of the valence band offset 278
(VBO). McKee et al. [15] argue that the most accu- 279
rate method for finding the VBM involves fitting a 280
theoretical VB density of states (VBDOS), calcu- 281
lated from density functional theory (DFT) and 282
convolved with a Gaussian to simulate the effects 283
of instrumental broadening, to the experimental 284
spectrum. The VBM is then equated with the en- 285
ergy at which the unbroadened VBDOS goes to 286
zero. This approach is the same as that originally 287
taken by Kraut et al. [16,17], who used this method 288
to find band offsets for HJs of more covalent semi- 289
conductors. In contrast, Chambers et al. [18,19] ar- 290
gue that DFT is not sufficiently accurate for this 291
task when applied to oxides, even though the pro- 292
cedure works very well for more covalent semicon- 293
ductors such as Si, Ge and III-Vs. We argue that a 294
more accurate method involves finding the inter- 295
cept between a line fit to the VB leading edge with 296
one fit to the background between the VBM and 297
the Fermi level—the so-called linear method 298
[18,19]. The error incurred by using Kraut's meth- 299
od with DFT theory is ∼0.5 eV for oxides such as 300
SrO, TiO$_2$ and SrTiO$_3$ [19]. We show that if a more 301
accurate self-consistent GW theory is used, agree- 302
ment between theory and experiment is much bet- 303
ter, and the difference between Kraut's method 304
and the linear method is within experimental 305
uncertainty (a few hundredths of an eV) [18]. 306
We draw similar conclusions here for α-Cr$_2$O$_3$ 307
and α-Fe$_2$O$_3$. We show in Fig. 4 fits of the experi- 308
mental VB spectra for α-Cr$_2$O$_3$ and α-Fe$_2$O$_3$ after 309
background subtraction (open circles) to VBDOS 310
generated by DFT (solid curves) in the generalized 311
gradient approximation (GGA). The raw VBDOS 312
have been broadened by convolution with Gaussi- 313
ans of width equal to 0.46 eV, the experimental 314
resolution used in these measurements. The bind- 315
ing energy scales are relative to the energies at 316

ARTICLE IN PRESS

Fig. 4. Valence band photoemission spectra (open circles) for epitaxial: (a) α-Fe$_2$O$_3$(0001), and (b) α-Cr$_2$O$_3$(0001), along with theoretical VBDOS (solid curve) computed from DFT GGA and broadened by convolving with a Gaussian of width equal to 0.46 eV to simulate instrumental resolution. The theoretical VBM is the energy at which the unbroadened theoretical VBDOS goes to zero. Also shown is the VBM determined by extrapolating the leading edge of the experimental VB spectrum to background.

which the unbroadened VBDOS go to zero, which are by definition the theoretical VBM for the two materials. The fit between broadened theory and experiment is not particularly good for either oxide. In both cases, the overall width of the VB is smaller in theory than in experiment, and the calculated VB leading edges rise more rapidly than their experimental counterparts. These two short-comings are most likely due to the fact that DFT predicts d-states that are too shallow relative to experiment due to the neglect of orbital-dependent exchange. As a result, the VBM found by the linear method is ~0.2 and ~0.5 eV higher in energy than that found by Kraut's method with DFT for α-Fe$_2$O$_3$ and α-Cr$_2$O$_3$, respectively. These results are similar to what was found earlier for SrTiO$_3$, TiO$_2$, and SrO [18,19]. For the same reasons as those elucidated in Refs. [18,19], we judge the linear method to be the more reliable method of obtaining the VBM of oxides in the absence of more accurate self-consistent GW calculations. Therefore, we corroborate earlier results [8] and

reaffirm that ΔE_v for α-Cr$_2$O$_3$ on α-Fe$_2$O$_3$(0001) and α-Fe$_2$O$_3$ on α-Cr$_2$O$_3$(0001) are +0.7 ± 0.1 and −0.3 ± 0.1 eV, respectively.

Another question mark surrounding the band offset analysis of HJs made from these materials has to do with the values of the bandgaps. Once ΔE_v is known, the conduction band offset is given by

$$\Delta E_c = \Delta E_g - \Delta E_v \qquad (2)$$

Here, ΔE_g is the difference in bandgaps for the two materials. In our prior analysis [8], we used band gaps derived from optical methods −4.8 ± 0.2 and 2.1 ± 0.1 eV for amorphous and polycrystalline films of α-Cr$_2$O$_3$ [20] and α-Fe$_2$O$_3$ [21], respectively. We note that optical methods may be influenced by the creation of bound excitons rather than true interband transitions leading to e$^-$/h$^+$ pairs, which are required to drive photochemistry in these materials. Photoconductivity is a better way to measure bandgaps because one can find the excitation energies at which free e$^-$/h$^+$ pairs are created, leading to an increase in conductivity at threshold. However, this method does not work well for materials with low-carrier mobility, such as the wide band gap semiconducting and insulating oxides in which we are presently interested.

In the present work we have employed two methods to determine bandgaps in our epitaxial films—optical absorbance and core-level photoelectron energy loss. We show in Fig. 5 optical absorbance spectra for thick epitaxial films of α-Cr$_2$O$_3$ and α-Fe$_2$O$_3$ grown on α-Al$_2$O$_3$(0001). The absorption onset for α-Fe$_2$O$_3$ is at ~2.2 eV, in good agreement with previous optical results [21]. However, in the absence of photoconductivity measurements, we cannot know if excitation at 2.2 eV represents the creation of bound excitons or unbound e$^-$/h$^+$ pairs. The onset of absorbance in the α-Cr$_2$O$_3$ spectrum falls at ~3.1 eV, well below the previously measured optical bandgap. By comparing these spectral data with those obtained with O 1s core-level photoemission energy loss, shown in Fig. 6, we suspect that this low-energy excitation corresponds to bound exciton creation. In the core-level spectrum, loss intensity associated with strong interband transitions above the optical

SUSC 15669

1 June 2005 Disk used

ARTICLE IN PRESS

No. of Pages 11, DTD = 5.0.1

SURFACE SCIENCE
LETTERS

S.A. Chambers et al. / Surface Science xxx (2005) xxx–xxx 7
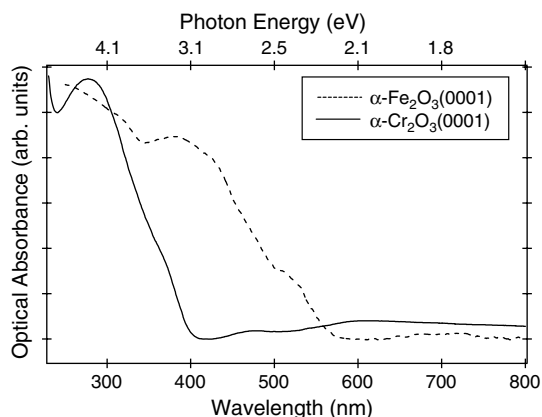
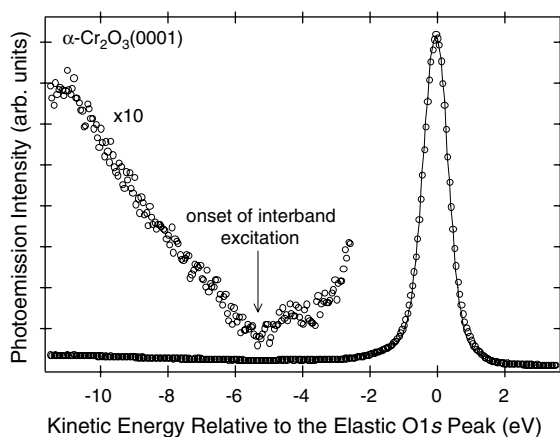Fig. 5. Optical absorbance spectra for epitaxial films of α-Cr$_2$O$_3$ and α-Fe$_2$O$_3$(0001).

Fig. 6. O 1s core-level XPS spectrum taken at normal emission for epitaxial α-Cr$_2$O$_3$(0001), including the energy loss region to low (high) kinetic (binding) energy from which the onset of interband excitation can be estimated.

387 bandgap of ∼4.8 eV is apparent. However, we also
388 see weaker loss features between ∼3 and ∼4.5 eV,
389 which we assign to bound exciton creation.
390 Partial densities of states projected onto Cr and
391 O sites in α-Cr$_2$O$_3$ reveal that the intense feature
392 between 0 and 1 eV binding energy in the VB spec-
393 trum of α-Cr$_2$O$_3$ (Fig. 4b) is ∼90% Cr 3d t_{2g} in
394 character. The multiple peak structure between 2
395 and 8 eV binding energy is primarily O 2p derived.
396 Additionally, we have been able to fit the complex
397 multiplet structure seen in the high-resolution Cr
398 2p core-level spectrum using an atomic multiplet

399 model by assuming a value of 10Dq of 2.5 eV,
400 which is in excellent agreement with the bulk value
401 [22]. Therefore, there are unoccupied Cr 3d e_g
402 states in the gap ∼1.5–2.5 eV above the VBM.
403 Excitation of VB electrons to unoccupied states
404 of Cr d character may account for the sub-band-
405 gap oscillator strength observed in the optical
406 spectrum of α-Cr$_2$O$_3$ (Fig. 5). Nevertheless, to
407 the best of our ability, we have confirmed that
408 bandgap assignments of ∼2.2 and ∼4.8 eV for α-
409 Fe$_2$O$_3$ and α-Cr$_2$O$_3$, respectively, are appropriate
410 for our epitaxial films. As a result, the CBO values
411 previously determined [8] are corroborated, and
412 both HJs can be described a being of the type II
413 or staggered band alignment.

4. Photochemistry of TMA 414

415 To evaluate heterogeneous photocatalytic activ-
416 ity at the surfaces of interest, we measured the ex-
417 tent of photodissociation of adsorbed TMA with
418 chopped Hg arc lamp UV light of $\lambda \geqslant 385$ nm.
419 Photodissociation of TMA on TiO$_2$ (1 1 0) rutile
420 has been studied in detail [1,23]. However, to the
421 best of our knowledge, similar experiments have
422 not been carried out on the α-Cr$_2$O$_3$ or α-
423 Fe$_2$O$_3$(0001) surfaces, or on heterojunctions made
424 from these materials. TMA is adsorbed by dosing
425 the sample with TMAA, which in turn undergoes
426 acid dissociation, leaving TMA bound to surface
427 cations and an acid proton bound to surface O lat-
428 tice anions. A schematic depiction of the photodis-
429 sociation process is shown in Fig. 7. TMA is likely
430 to sorb in a monodentate fashion, since the cation-
431 cation spacing is too large for bidentate coordina-
432 tion of the carboxyl functional group. TMA acts
433 as a hole acceptor, resulting in photodissociation
434 into CO$_2$ and one of several other possible molec-
435 ular fragments, as shown in Fig. 7. By using light
436 of $\lambda \geqslant 385$ nm ($h\nu \leqslant 3.2$ eV), no absorption lead-
437 ing to e$^-$/h$^+$ pair creation is expected in the α-
438 Cr$_2$O$_3$ layer, which is the top layer in these exper-
439 iments. However, since 3.2 eV exceeds the band-
440 gap of α-Fe$_2$O$_3$, e$^-$/h$^+$ pairs should be created in
441 the buried α-Fe$_2$O$_3$ layer. In principle, the holes
442 should diffuse to the α-Cr$_2$O$_3$ layer, since their en-
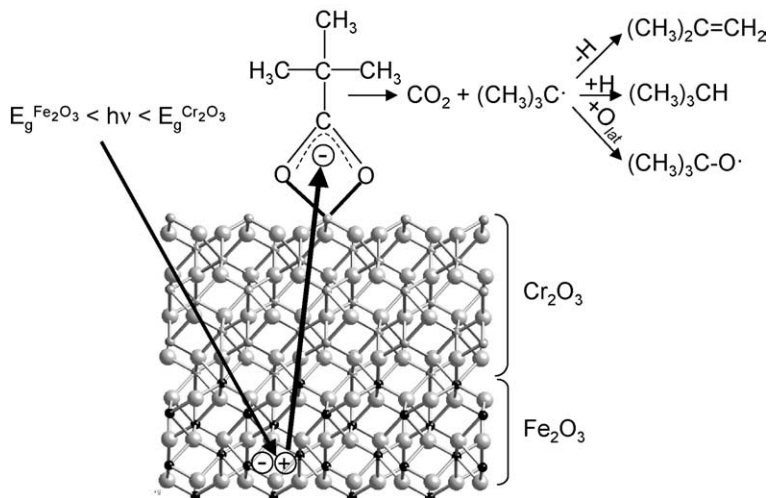
S.A. Chambers et al. / Surface Science xxx (2005) xxx–xxx

Fig. 7. Schematic drawing depicting the chemisorption of TMA at cation sites on a α-Cr$_2$O$_3$/α-Fe$_2$O$_3$ heterojunction surface, the absorbance of UV light of photon energy less than that of α-Cr$_2$O$_3$ but greater than that of α-Fe$_2$O$_3$, hole diffusion to the α-Cr$_2$O$_3$ surface, and hole-mediated photodecomposition of TMA to CO$_2$ and a butyl radical. Subsequent reactions of the butyl radical with acid protons (from dissociation of TMAA) or lattice oxygens are also shown.

ergy is lower there, whereas the electrons should remain in the buried α-Fe$_2$O$_3$ layer.

We show in Fig. 8 high-resolution C and O 1s core-level spectra obtained at a take-off angle (θ_t) of 12° for saturation doses of TMAA for thick-films of α-Fe$_2$O$_3$ and α-Cr$_2$O$_3$(0001), along with those of HJs in which the top layer was α-Cr$_2$O$_3$. All surfaces were at 300 K during dosing. The C 1s spectra consist of two peaks, one for aliphatic carbon at ~284.5 eV, and one for carboxyl carbon at ~288.3 eV. The O 1s spectra exhibit an intense lattice oxygen peak at 530.0 eV, and a carboxyl
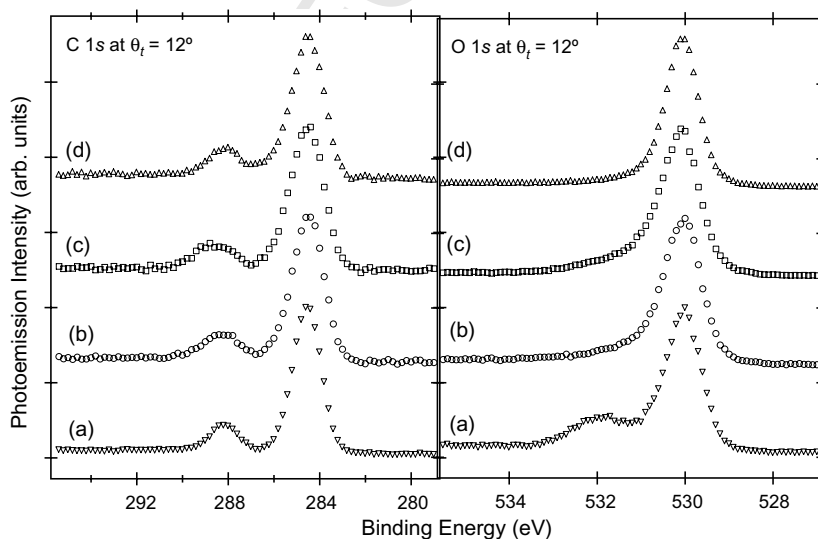

Fig. 8. C 1s (left) and O 1s (right) core-level spectra obtained at a take-off angle (θ_t) of 12° for saturation doses of TMA on (a) α-Fe$_2$O$_3$(0001), (b) 2 ML α-Cr$_2$O$_3$/α-Fe$_2$O$_3$(0001), (c) 10 ML α-Cr$_2$O$_3$/α-Fe$_2$O$_3$(0001), and (d) 350 ML α-Cr$_2$O$_3$/α-Fe$_2$O$_3$(0001).

9

455 peak at ∼532 eV, which is clearly visible only
456 on the pure α-Fe$_2$O$_3$(0001) surface. TMA on
457 α-Cr$_2$O$_3$(0001), in either thick or thin film form,
458 results in a much weaker carboxyl O 1s feature
459 with a smaller chemical shift relative to the lattice
460 O peak. The spectra have been normalized to a
461 constant height. Therefore, it is not apparent from
462 Fig. 8 that TMA uptake is much greater on α-
463 Fe$_2$O$_3$ than on α-Cr$_2$O$_3$. We estimate the absolute
464 TMA coverage on the various surfaces the follow-
465 ing way. Starting with the α-Fe$_2$O$_3$(0001) surface,
466 we reference the carboxyl O 1s peak area to the lat-
467 tice O 1s peak area by noting that the lattice O 1s
468 intensity can be written as

$$I_{\text{lat}}(\theta_t) = \sum_j I_j(\theta_t) = I_o \sum_j \exp(-d_j/\lambda \sin \theta_t) \quad (3)$$

472   Here, we sum over layers of closed-packed O
473 anions assuming a continuum model for the mate-
474 rial characterized by an electron attenuation
475 length, λ, and O layer depths below the surface
476 of d_j. Photoelectron diffraction effects are ignored.
477 I_o is the O 1s intensity from the topmost layer of O
478 anions. The TMA carboxyl O 1s peak intensity
479 after sorption on α-Fe$_2$O$_3$(0001) can be written as,

$$I_{\text{TMA}}(\theta_t) = fI_o \qquad (4)$$

483 where f is the TMA oxygen fractional coverage in
484 units of a ML of close-packed lattice O. Combin-
485 ing Eqs. (3) and (4) yields,

$$\ln(f) = \ln \sum_j \exp(-d_j/\lambda \sin \theta_t) \\ + \ln[I_{\text{TMA}}(\theta_t)/I_{\text{lat}}(\theta_t)] \qquad (5)$$

488   The first term on the right is computed for rea-
489 sonable values of attenuation length, and the sec-
490 ond term contains the measured peak areas from
491 the O 1s spectrum for α-Fe$_2$O$_3$(0001). The TMA
492 coverage referenced to the cation density on the
493 surface of α-Fe$_2$O$_3$(0001), $\Theta_{\text{TMA}}^{\text{Fe}_2\text{O}_3}$, is then
494 3.0(0.5f) = 1.5f. Here, we note that the factor of
495 0.5 stems from the fact that there are two oxygens
496 per TMA anion, and the factor of 3.0 from the fact
497 that the α-Fe$_2$O$_3$(0001) surface is terminated with
498 1/3 ML of Fe cations [12]. Finally, the TMA cov-
499 erage on the α-Cr$_2$O$_3$(0001) surface, $\Theta_{\text{TMA}}^{\text{Cr}_2\text{O}_3}$, can
500 be related to $\Theta_{\text{TMA}}^{\text{Fe}_2\text{O}_3}$ by the formula,

$$\Theta_{\text{TMA}}^{\text{Cr}_2\text{O}_3} = \Theta_{\text{TMA}}^{\text{Fe}_2\text{O}_3}[I_{\text{C 1s}}^{\text{Cr}_2\text{O}_3}(\theta_t)/I_{\text{C 1s}}^{\text{Fe}_2\text{O}_3}(\theta_t)] \qquad (6)$$

where $I_{\text{C 1s}}^{\text{Cr}_2\text{O}_3}(\theta_t)$ and $I_{\text{C 1s}}^{\text{Fe}_2\text{O}_3}(\theta_t)$ are the total C1s areas 503
under both aliphatic and carboxyl peaks on the α- 504
Cr$_2$O$_3$(0001) and α-Fe$_2$O$_3$(0001) surfaces, respec- 505
tively. Using $\lambda = 12 \pm 3$ Å, we arrive at $\Theta_{\text{TMA}}^{\text{Fe}_2\text{O}_3} =$ 506
1.1 ± 0.2 ML and $\Theta_{\text{TMA}}^{\text{Cr}_2\text{O}_3} = 0.3 \pm 0.2$ ML. The 507
lower TMA coverage on the α-Cr$_2$O$_3$(0001) 508
surfaces is most likely due to a partial chromyl ter- 509
mination [13], which is expected to block cation 510
sites from chemisorption of other species at 511
300 K [24]. We draw this conclusion based on 512
the fact that subsequent UHV annealing of the 513
α-Cr$_2$O$_3$(0001) to drive off the TMA, followed by ç
readsorption of TMAA, invariably results in an in- 515
crease in TMAA uptake, presumably as a result of 516
removal of some of the chromyl termination. 517

We now examine the photodesorption products 518
of TMA from these different surfaces. We moni- 519
tored mass 44 (CO$_2$), 41 (C$_3$H$_5$—a mass fragment 520
common to all three final products depicted in Fig. 521
7), and mass 18 (H$_2$O) as a function of time before, 522
during and after a 60 s UV light exposure at 523
$\lambda \geqslant 385$ nm, with the surface at 300 K. The result-
ing traces typically look like that shown in Fig. 9, 525
which were taken for 10 ML α-Cr$_2$O$_3$ on α- 526
Fe$_2$O$_3$(0001). Masses 44 and 41 rise as soon as 527
the light shutter is opened at $t = 0$, and either 528
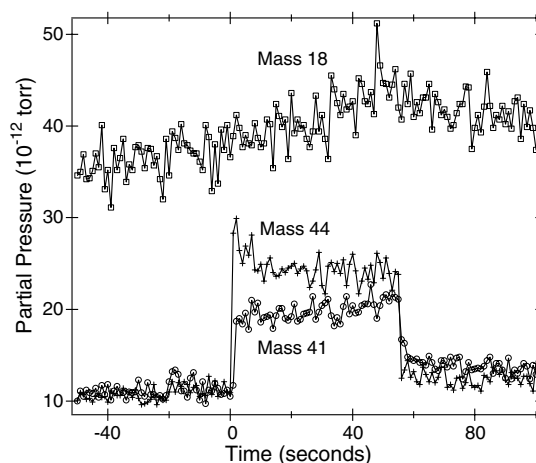slightly decay, or remain constant during the irra- 529

Fig. 9. Desorption yields for masses 18, 44, and 41 from 10 ML α-Cr$_2$O$_3$/α-Fe$_2$O$_3$(0001) using chopped Hg arc lamp UV light with a 385 nm cut-off filter.

diation period, and then drop immediately when the light shutter is closed. The instantaneous response indicates that these are photodesorption as opposed to thermal desorption products. In contrast, the mass 18 peak rises slowly after opening the light shutter, as expected for a thermal desorption product arising from UV heating of the sample. The lack of signal fall off throughout light exposure for masses 41 and 44 is most likely due to accumulation of charge as a result of the insulating nature of these materials, as well as a slight thermal contribution due to sample heating. Internal charging in the surface or HJ is expected if the TMA scavenges the holes, and the material is not sufficiently conductive to conduct away the electrons.

The dependence of the extent of photodesorption on α-Cr$_2$O$_3$ layer thickness in HJs is shown in Fig. 10. Here we plot the mass 44 signal, normalized to the amount of TMA on the surface, vs. time for: (a) thick-film α-Fe$_2$O$_3$(0001), (b) 2 ML α-Cr$_2$O$_3$, (c) 10 ML α-Cr$_2$O$_3$, and (d) 350 ML α-Cr$_2$O$_3$, all on thick-film α-Fe$_2$O$_3$(0001). The photoresponse of the α-Fe$_2$O$_3$(0001) surface is rather slight, even though the UV light energy exceeds the bandgap. Nonradiative recombination of

e^-/h^+ pairs at the surface or hole trapping in d states in the gap may be responsible for this result. Moving to the HJs, the photoresponse is larger for 2 and 10 ML of α-Cr$_2$O$_3$ on α-Fe$_2$O$_3$(0001) than it is for pure α-Fe$_2$O$_3$, and the response is approximately the same for these two HJs. Taken at face value, this result suggests that the HJ promotes hole-mediated decomposition of TMA, possibly through e^-/h^+ pair separation via a staggered band alignment. In order to test this idea, we examine the photoresponse of a much thicker α-Cr$_2$O$_3$ layer (350 ML, or ∼800 Å). In this case, the light is expected to penetrate to the buried HJ where it will be absorbed. However, it is not anticipated that the hole will be able to readily diffuse to the surface because of the very high resistivity of epitaxial α-Cr$_2$O$_3$. Surprisingly, a photoresponse is still present at 350 ML (Fig. 10d). This result reveals that an excitation leading to photochemical decomposition of TMA is able to occur, even though the UV light energy is less than the bandgap of α-Cr$_2$O$_3$. One way this phenomenon could happen is through creation of a bound exciton at the surface which affects the stability of the bonds in the TMA species. As seen in Fig. 5, there is weak optical absorption in α-Cr$_2$O$_3$ at 385 nm, presumably due to dipole allowed O 2p to Cr 3d or weak Cr d–d transitions that become allowed by admixture with O 2p states. Both transitions are expected to lead to bound exciton formation. Inasmuch as these excitations change the valence electron distribution in surface Cr cations, the C–C bond in TMA between the t-butyl and carboxylate groups may be weakened to the point that decomposition occurs. This unexpected and interesting result will be more thoroughly explored in future work.
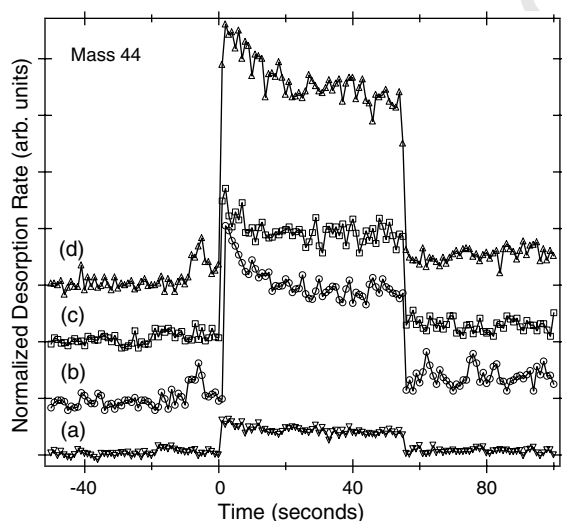
5. Summary

We have investigated the possibility that electron–hole pair creation and separation, via staggered band alignment at an oxide/oxide heterojunction, might enhance photochemical decomposition of an adsorbed molecule. Our test case was hole-mediated photodecomposition of trimethyl acetate on well-defined epitaxial heterojunctions of α-Cr$_2$O$_3$(0001) on α-Fe$_2$O$_3$(0001)

Fig. 10. Mass 44 photodesorption yield using chopped Hg arc lamp UV light with a 385 nm cut-off filter for (a) α-Fe$_2$O$_3$(0001), (b) 2 ML α-Cr$_2$O$_3$/α-Fe$_2$O$_3$(0001), (c) 10 ML α-Cr$_2$O$_3$/α-Fe$_2$O$_3$(0001), and (d) 350 ML α-Cr$_2$O$_3$/α-Fe$_2$O$_3$(0001).

601 using UV light of energy intermediate between the
602 bandgaps of the two oxides. There is no obvious
603 effect of the staggered band alignment on the pho-
604 tochemical process. Rather, photochemical
605 decomposition is more extensive on α-Cr_2O_3, for
606 which the exciting light is not sufficiently energetic
607 to create electron–hole pairs, than it is on α-Fe_2O_3,
608 for which the light energy exceeds the bandgap.
609 We suggest that this interesting and unanticipated
610 effect may be driven by the creation of bound exci-
611 tons which lead to photodecomposition of the
612 adsorbate. We plan to investigate this phenome-
613 non in more detail in the future.

631 **References**

632 [1] J.M. White, J. Szanyi, M.A. Henderson, J. Phys. Chem. B.
633   107 (2003) 2009.

[2] See, for example M. Anpo, M. Takeuchi, J. Catal. 216
    (2003) 505.
[3] S. Thiel, T. Kluner, M. Wilde, K. Al-Shamery, H.J.
    Freund, Chem. Phys. 228 (1998) 185.
[4] J. Bandara, J.A. Mielczarksi, A. Lopez, J. Kiwi, Appl.
    Catal. B—Environ. 34 (2001) 321.
[5] M.A. Gondal, A. Hameed, Z.H. Yamani, A. Suwaiyan,
    Appl. Catal. A—Gen. 268 (2004) 159.
[6] J. Shang, Y.F. Zhu, Z.L. Xu, L.Q. Jing, Y.G. Du, Chinese
    J. Catal. 24 (2003) 369.
[7] S. Sakthivel, S.-U. Geissen, D.W. Bahnemann, V. Muruge-
    san, A.J. Vogelpohl, J. Photochem. Photobiol. A 148
    (2002) 283.
[8] S.A. Chambers, Y. Liang, Y. Gao, Phys. Rev. B. 61 (2000)
    13223.
[9] J.E. Jaffe, M. Dupuis, M. Gutowski, Phys. Rev. B. 69
    (2004) 205106.
[10] A. Francioso, C.G. Van de Walle, Surf. Sci. Rep. 25 (1996)
    1.
[11] S.A. Chambers, Surf. Sci. Rep. 39 (2000) 105.
[12] S.A. Chambers, S.I. Yi, Surf. Sci. 439 (1999) L785.
[13] B. Dillmann et al., Faraday Discuss. 105 (1997) 295.
[14] S.A. Chambers, The chemical physics of solid surfaces, in:
    D.P. Woodruff (Ed.), Oxide Surfaces, vol. 9, Elsevier,
    Amsterdam, 2001 (Chapter 7).
[15] R.A. McKee, F.J. Walker, M.B. Nardelli, W.A. Shelton,
    G.M. Stocks, Science 300 (2003) 1726.
[16] E.A. Kraut, R.W. Grant, J.R. Waldrop, S.P. Kowalczyk,
    Phys. Rev. Lett. 44 (1980) 1620.
[17] E.A. Kraut, R.W. Grant, J.R. Waldrop, S.P. Kowalczyk,
    Phys. Rev. B 28 (1983) 1965.
[18] S.A. Chambers, T. Droubay, T.C. Kasper, M. Gutowski,
    M. van Schilfgaard, Surf. Sci. 554 (2004) 81.
[19] S.A. Chambers, T. Droubay, T.C. Kasper, M. Gutowski,
    J. Vac. Sci. Technol. B 22 (2004) 2205.
[20] S. Hong, E. Kim, D.-W. Kim, T.-H. Sung, K. No, J. Non-
    Cryst. Sol. 221 (1997) 245.
[21] S. Mohanty, J. Ghose, J. Phys. Chem. Solids 53 (1992) 81.
[22] S.A. Chambers, T. Droubay, Phys. Rev. B 64 (2001)
    075410.
[23] M.A. Henderson, J.M. White, H. Uetska, H. Onishi, J.
    Amer. Chem. Soc. 125 (2003) 14974.
[24] M.A. Henderson, S.A. Chambers, Surf. Sci. 449 (2000)
    135.